

EGFN: Efficient Geometry Feature Network for Fast Stereo 3D Object Detection

Aqi Gao, Yanwei Pang, Jing Nie, Jiale Cao and Yishun Guo
Tianjin University

gaoaqi, pyw, jingnie, connor, guoyishun@tju.edu.cn

Abstract

Fast stereo based 3D object detectors have made great progress in the sense of inference time recently. However, they lag far behind high-precision oriented methods in accuracy. We argue that the main reason is the missing or poor 3D geometry feature representation in fast stereo based methods. To solve this problem, we propose an efficient geometry feature generation network (EGFN). The key of our EGFN is an efficient and effective 3D geometry feature representation (EGFR) module. In the EGFR module, light-weight cost volume features are firstly generated, then are efficiently converted into 3D space, and finally multi-scale features enhancement in both image and 3D spaces is conducted to obtain the 3D geometry features: enhanced light-weight voxel features. In addition, we introduce a novel multi-scale knowledge distillation strategy to guide multi-scale 3D geometry features learning. Experimental results on the public KITTI test set shows that the proposed EGFN outperforms YOLOStereo3D, the advanced fast method, by 5.16% on mAP_{3d} at the cost of merely additional 12 ms and hence achieves a better trade-off between accuracy and efficiency for stereo 3D object detection. Our code will be publicly available.

1. Introduction

3D object detection is an important and fundamental task for many applications such as automatic driving, service robot and so on. Though LiDAR-based 3D object detection approaches [22, 23, 26] have high accuracy, they suffer from the expensive hardware cost and low resolution. Compared with LiDAR-based 3D object detection approaches, stereo-based 3D object detection approaches [14, 19, 33] adopt the low-cost optical cameras and can provide dense 3D information. In this paper, we focus on stereo-based 3D object detection. The stereo-based 3D object detection approaches can be mainly divided into image space based methods [14, 17, 19, 30], pseudo LiDAR based methods [10, 11, 20, 31, 33, 40], and voxel based methods [3, 5].

Because object detection efficiency is of great impor-

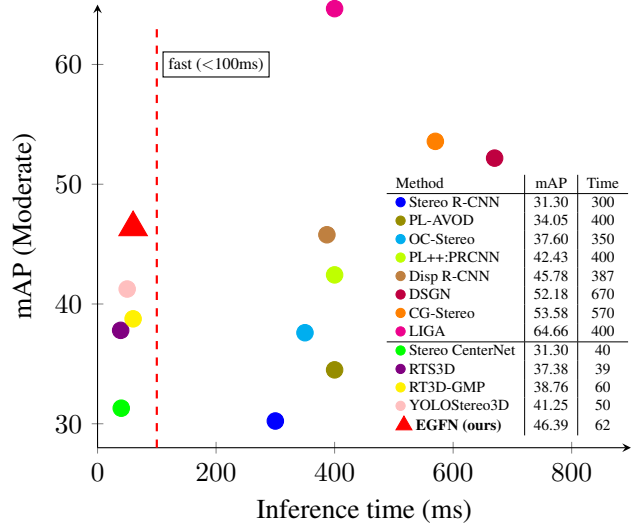


Figure 1. Accuracy (mAP) and inference time (ms) comparison of some state-of-the-art stereo 3D object detection methods on KITTI test (moderate) set [4]. The inference time of most methods, except YOLOStereo3D [17], are taken from the leaderboards in the official KITTI website, due to no source codes. The inference time of YOLOStereo3D and our EGFN are reported on NVIDIA RTX 3090 for a fair comparison. Overall, our EGFN achieves a state-of-the-art trade-off between accuracy and speed.

tance for real-time applications such as automatic driving, it is crucial develop fast stereo 3D object detection methods. Recently, the researchers started to focus on fast stereo 3D object detection. As shown in Fig. 1, we define fast stereo 3D object detection as the methods with the detection time less than 100ms. Most of these fast methods belong to either image space based methods (e.g., YOLOStereo3D [17] and Stereo CenterNet [30]) or pseudo LiDAR based methods (e.g., RT3D-GMP [11] and RT3DStereo [10]). The image space based methods (see Fig. 2(a)) use features in image space to perform 3D object detection. Pseudo LiDAR based methods obtain the depth map by a fast depth estimation module and transform it into point cloud. After that, they employ a light-weight point cloud detector to detect objects. These fast stereo 3d object detection approaches

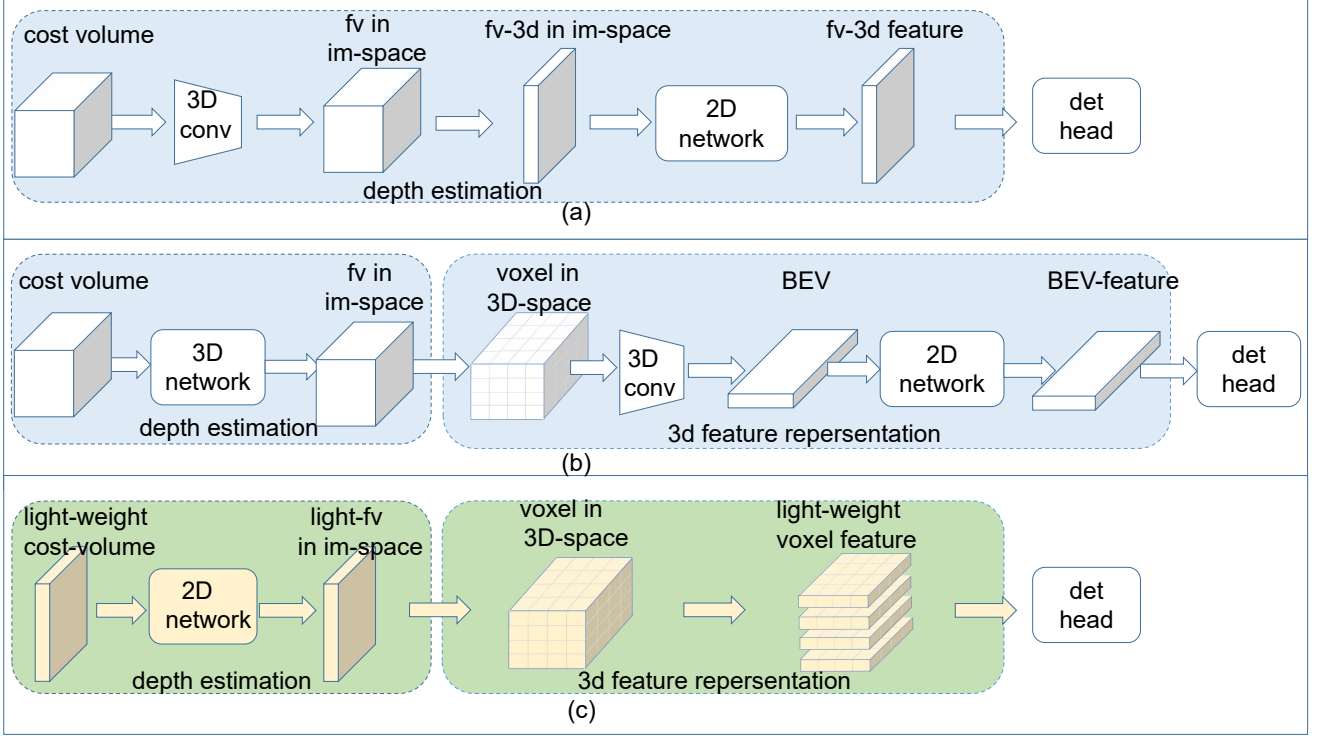


Figure 2. The pipelines of stereo based detectors, most of them are consisted of depth estimation module and 3D feature presentation module. The pipeline of YOLOStereo3D [17] is (a), which first construct 4D cost volume with a little channel numbers, second the cost volume is aggregated by a 3D convolution to get a feature volume(fv), third fv is compressed to three-dimension and is processed by 2D network, finally fv feature is sent to detection head. The pipeline of DSGN [3] is (b), the detail of it will be introduced in Sec. 3.1, it uses a number of 3D convolution and aggregation networks. The pipeline of our method is (c), the detail of it will be introduced in In Sec. 3.2.

usually adopt the light-weight modules in each processing step as possible, which greatly improves the speed. However, these methods are inferior in accuracy.

Compared with these fast stereo based methods, voxel based methods [3, 5] are superior in accuracy. Fig. 2(b) shows the basic pipeline of them. They first use a heavy 3D network to generate a feature volume (fv) in image space. After that, they transform the fv in image space to 3D space and perform 3D convolution. Finally, they rearrange it into 2D bird’s eye view (BEV) and employ a 2D Hourglass network to aggregate BEV feature. Due to these complicate operations on 3D representation, voxel based methods are very slow and can not meet the need of practical application.

We argue that, compared with voxel based methods, the poor accuracy of fast stereo based methods are due to the lack of good 3D scene representation features. To solve the problem, we propose an efficient and effective 3D geometry feature representation module called EGFR. The basic block is shown in Fig. 2(c). We first build a light-weight 3D cost volume instead of the time-consuming 4D cost volume. Different from the 3D aggregation network in

Fig. 2(b), we only use a light-weight 2D aggregation network to get a light-fv in image space. Second, we transform the light-fv into 4D fv temporarily, project it into 3D space, and directly compress it into light-weight voxel feature without any other intermediate processing. After that, we perform multi-scale features enhancement to obtain the efficient and effective 3D geometry features: enhanced light-weight voxel features. With our proposed module EGFR, we construct a fast stereo 3D object detector, called EGFN. Compared to high-accuracy stereo method DSGN in Fig. 2(b), our EGFR does not require any 3D convolution operation and complicate cumbersome aggregation networks. Compared to fast stereo method YOLOStereo3D, our EGFR generates 3D geometry feature in 3D space and avoids object distortion in image space.

Furthermore, we introduce a new multi-scale knowledge distillation strategy. Specifically, we employ a new LiDAR-based network and train this network with inputting accurate 3D point cloud. After that, the LiDAR-based network is used as the teacher to guide multi-scale features learning in our stereo objector EGFN. We perform the experiments on the typical KITTI dataset. As shown in Fig. 1, our proposed

EGFN achieves an optimal trade-off between accuracy and speed. Our contributions can be summarized as follows:

- We propose an efficient geometry feature network (EGFN) fast stereo 3D object detection. The key module is a light-weight 3D feature generation module EGFR. The EGFR module is able to efficiently and effectively generates rich 3D geometry features in 3D space without any 3D convolution.
- We introduce a new multi-scale distillation strategy to enhance the 3D geometry features by customizing a new LiDAR-based teacher module to provide multi-scale 3D features supervision.
- We perform experiments on KITTI dataset. Our approach achieves 46 moderate mAP on the official KITTI benchmark at the speed of 62ms per frame, obtaining an optimal trade-off in terms of accuracy and speed.

2. Related Work

2.1. 3D point cloud object detection

3D point cloud object detection is crucial for automatic driving. The methods of point detection can be mainly divided into three parts: voxel based, point based, Point-voxel-based. Voxel based methods [12, 28, 39, 43] change the irregular point clouds to the volumetric representations in compact shape to efficiently extract point features for detection. Some backbones (*e.g.*, PointNet [22] and PointNet++ [23]) are proposed to extract the features from the point cloud. Based on these, point-based 3D detectors [21, 27, 29, 34, 37] are proposed to detect objects by using point cloud directly. However, voxel-based methods are limited to the size of voxel, and point-based methods are high time-consuming to deal with irregular points. Point-voxel based methods [2, 6, 25, 38] can well tackle this problem so become a new trend recently.

2.2. Stereo 3D object detection

Stereo 3D object detection mainly consists of three classes: image space based methods, pseudo LiDAR based methods, voxel based methods. Image space based methods use features in the image coordinate system to achieve 3D object detection. Stereo-RCNN [14] generates a rough 3D bounding box by combining the RoIs from the left and right images and conducts BA optimization for final 3D bounding box prediction. IDA-3D [19] builds a cost volume from left and right ROIs to get the depth of the center point for 3D detection.

Pseudo LiDAR based methods need parallax and other supervision information. Pseudo-LiDAR [33] transforms

the depth map into a point cloud and performs 3D point cloud detection. Pseudo-LiDAR++ [40] proposes a depth cost volume to get a depth map directly. OC-Stereo [20] and Disp RCNN [31] only consider point cloud of the foreground regions. ZoomNet [35] improves the disparity estimation by enlarging the target region.

Different from the pseudo LiDAR based methods transforming the depth map into points, voxel-based methods use voxel features to detect objects directly. DSGN [3] converts an image volume to a space volume that represents the 3D geometry structure better. LIGA [5] applies a LiDAR detection model as a teacher model and makes a break through in accuracy. However, due to a large number of 3D convolutions and cumbersome pipelines, these methods are not fast enough to be applied in practice. Although some other works [10, 11, 15, 17, 30] have achieved high-speed inference, their accuracy can not meet the actual needs.

2.3. Knowledge Distillation

Knowledge distillation was first proposed by Hinton et al. [9] for model compression. A large teacher network provides “softened labels” for supervising a student network, so the student network can get better results. After that, [8, 24] makes use of knowledge from intermediate layers of teacher networks, which provides richer information. Recently, knowledge distillation has been successfully applied to stereo 3D object detection [5] and has obtained competitive results, which shows that effective feature imitation methods from LiDAR-based detectors to stereo-based detectors are of great importance.

3. Method

In this section, we provide a detailed introduction about our proposed network, called EGFN. The overall pipeline of our method is shown in the Fig. 3. We adopt the efficient model ResNet-34 [7] to extract multi-scale feature maps for the stereo input images. Based on these feature maps, we propose EGFR module to efficiently generate 3D geometry features: light-weight voxel features. Then a teacher LiDAR detector module provides multi-scale 3D feature imitation to enhance the light-weight voxel features leaning more accurate 3D geometry information. Finally, the enhanced 3D features are sent to the detection heads to obtain the detection results. We first revisit existing 3D feature generation module in Sec. 3.1, which is helpful for understanding our method. In Sec. 3.2, we introduce the details of the proposed efficient 3D geometry feature representation (EGFR) module. Sec. 3.3 describes the multi-scale feature distillation module in which a new LiDAR detector is designed to provide multi-scale 3D feature imitation to enhance our light-weight voxel features. Finally, the 3D detection head and the depth head are presented in Sec. 3.4.

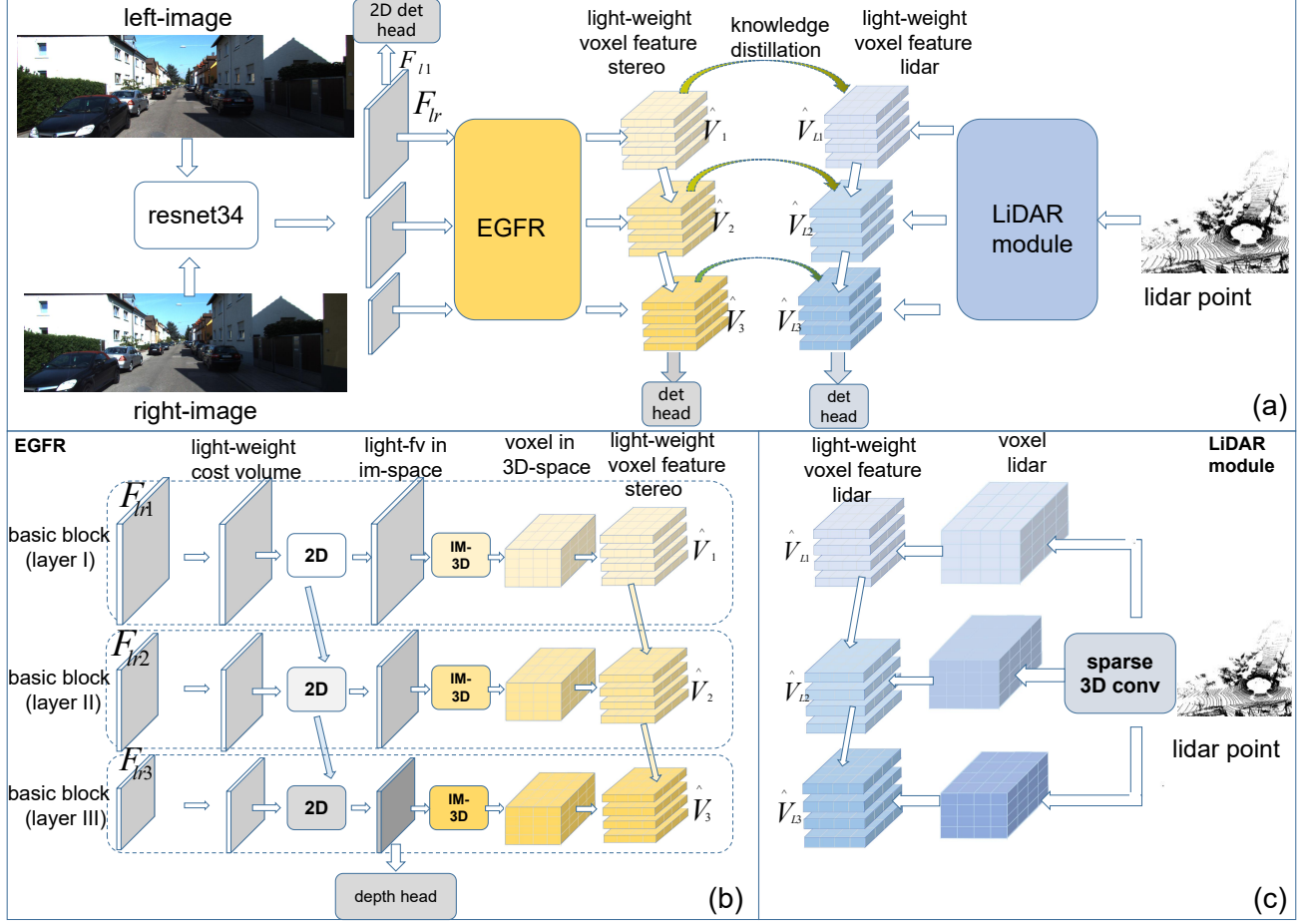


Figure 3. Overall architecture of our proposed EFGN for fast stereo 3D object detection. For the stereo input images, we adopt the efficient deep model ResNet-34 [7] to extract multi-scale feature maps. Based on these feature maps from left and right images, we propose a novel EGFR module to quickly generate multi-scale 3D geometry features. Moreover, we introduce a LiDAR detector to provide multi-scale feature imitation, which results in a better 3D geometry feature representation. Finally, the 3D geometry features are fed to the detection head to obtain 3D object detection results.

3.1. Existing 3D Feature Generation Module

Firstly, we revisit the 3D feature generation pipeline proposed in the existing high-precision stereo 3D detection methods [3, 13]. As shown in Fig. 2(b) the left-right features (F_l , F_r) obtained through the backbone will first construct a 4D cost volume from Eq. 1.

$$csv(u, v, i) = cat[F_l(u, v), F_r(u - fb/dep(i), v)], \quad (1)$$

where i is depth index, $dep(i)$ is the depth, (u, v) is the current pixel coordinate, f is the camera focal length, and b is the baseline of the stereo camera pair.

Then the 4D cost volume are aggregated by a 3D hourglass network. The network is composed of a large number of 3D convolutions to obtain a feature volume. The feature volume is input to two branches: one is for depth regression and the other is to rearranged the features into 2D

bird’s eye view (BEV) features. An additional 2D hourglass network is attached to the BEV features to generate the aggregated BEV features for final detection. These pipelines need a large number of 3D convolution layers and a complex model to obtain the final features in 3D space for detection. So these methods are inefficient.

3.2. EGFR module

We propose an efficient 3D geometry feature representation (EGFR) module to obtain features in 3D space efficiently. The EGFR module can be mainly divided into two parts: basic block and multi-scale enhancement.

Basic Block As shown in Fig. 3 (b), after getting feature maps from the backbone ResNet34, we will follow [18] and [32] to construct a light-weight cost volume (lcsv) by concatenating left features (F_l) and corresponding right

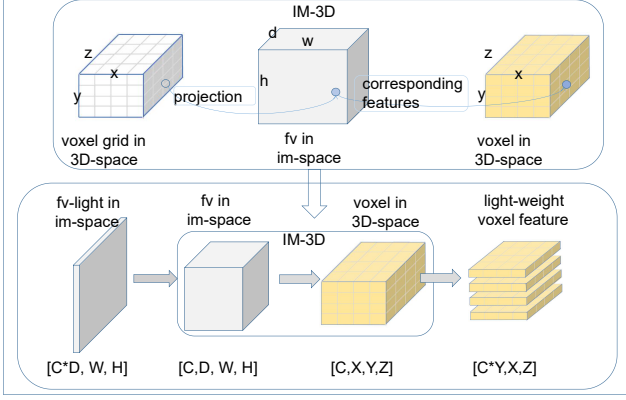


Figure 4. The structure of IM-3D. First, the light feature volume light-fv in im-space is temporarily converted into 4D, and next we project it to voxel in 3D space by using voxel grid. Then voxel will be directly compressed into light-weight voxel features.

features(F_r) according to the Eq. 2.

$$lcsv(u, i : V, i) = \frac{1}{C} \sum_c (F_l(u, i : V) * F_r(u, 0 : V - i)), \quad (2)$$

where i is depth index (0,1,2,...), (u, v) is the current pixel coordinate, V is maximal v , C means the channel numbers of features. Since the generated light-weight cost volume is three-dimensional, we only need a simple network with 2D convolutions to aggregate the cost volume and get a light feature volume (light-fv) in image space.

We apply an IM-3D module to transform the light-fv into voxels in 3D space. Fig. 4 shows the structure of the IM-3D module. The light-fv is temporarily converted into 4D and then be projected into voxels in 3D space by using voxel grid in 3D-space. Finally, we directly compress the voxels in 3D space into light-weight voxels, by merging c and y channel without using any 3D convolution and additional aggregated networks.

Multi-scale Enhancement For the basic block, we further conduct multi-scale enhancement to improve the light-weight voxels. We enhance the voxels at three scales: $1/2$, $1/4$, $1/8$ (recorded as I, II and III layer respectively). Multi-scale enhancement is employed in two aspects: On the one hand, we conduct multi-scale enhancement in light-fv of the image space to help improve depth estimation and obtain more accurate light-fv features. On the other hand, in terms of light-weight voxel features in 3D space, multi-scale enhancement is carried out to obtain more efficient 3D features: enhanced light-weight voxels.

(1) Multi-scale enhancement in the light-fv: we adopt the the Eq.3 to get enhanced light-fv, where $conv2D$ is a 2D convolution, cat is the operation of concatenation, $avgp$ means average pooling. The light-weight feature volume of layer I (light-fv₁) is down sampled to $1/4$, next concate-

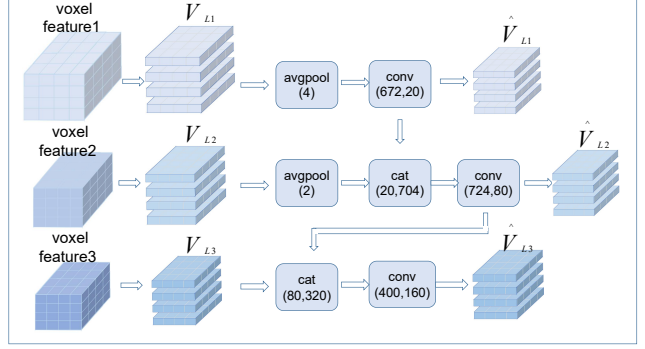


Figure 5. The details of multi-scale geometry feature enhancement based on a novel LiDAR detector, where avgpool represents average pool operation, cat represents concatenation operation, and conv represents 2D convolution operation.

nate with the light weight cost volume of layer II ($lcsv_2$), then passed through the 2D aggregation network to get the light-fv₂. Similarly, we get the light-fv₃ and we only add depth prediction head to light-fv₃. The channel number of features light-fv₁ and light-fv₂ is less, so as to ensure our high inference speed.

$$\begin{cases} lf_{v1} = conv2D(lcsv_1), \\ lf_{v2} = conv2D(cat(avg_{s2}(lf_{v1}), lcsv_2)), \\ lf_{v3} = conv2D(cat(avg_{s2}(lf_{v2}), lcsv_3)). \end{cases} \quad (3)$$

(2) Multi-scale enhancement in the light-weight voxel feature:

In the process of converting different scales light-fv _{i} ($i=1,2,3$) to the light-weight voxel features V_i , we use the same size of voxel grids to ensure that the converted voxel features V_i have the same resolution, which can improve the speed. After getting the same resolution light-weight voxel features V_i , we adopt the following steps to get multi-scale enhanced light-weight voxel features (\hat{V}_i):

$$\begin{cases} \hat{V}_1 = conv2D(V_1), \\ \hat{V}_2 = conv2D(cat(\hat{V}_1, V_2)), \\ \hat{V}_3 = conv2D(cat(\hat{V}_2, V_3, IMV_{oxel})), \end{cases} \quad (4)$$

where $conv2D$ is a 2D convolution, cat is the operation of concatenation, IMV_{oxel} is obtained by projecting the image feature F_{l1} out from the backbone into 3D space using the same voxel grid. Then, the enhanced multi-scale light-weight voxel feature \hat{V}_3 is sent to detection head for detection.

3.3. Multi-Scale 3D Feature Imitation

At present, the detection accuracy of LiDAR-based detectors is much better than that of stereo detectors. This is mainly due that LiDAR-based detectors can get better 3D features from the point cloud that has more accurate 3D information of itself. Point cloud itself has also been directly

used to supervise stereo detectors [17, 31] for a long time. But the learning effect is not satisfying because 3D features are affected by the inaccurate depth estimation in stereo detectors. Guo *et al.* [5] creatively proposed to use the multi-channel 3D features of middle layers in the LiDAR model to provide supervision for the stereo detector, which makes the stereo detector learn high-level geometry-aware 3D features and achieve the state-of-the-art results.

Inspired by [5], we customize a new LiDAR-based detector as a teacher to provide multi-scale 3D features imitation and guide our stereo module to learn better 3D geometry features. The main structure of our LiDAR model is shown in the right part of Fig. 3 (c). Firstly, the raw point cloud is voxelized into volumetric representations. The voxels then pass through a sparse 3D convolutional backbone to extract voxel features. The voxel features with the shape of (C, X, Y, Z) in each scale are reshaped as the voxel features $V_{L,i}$ ($i = 1, 2, 3$) with the shape of (CY, X, Z) , separately. Just like multi-scale enhancement in the light-fv (The detail is shown in Fig. 5), we perform multi-scale enhancement to get the final light-weight voxel features $\hat{V}_{L,i}$. Specially, the steps are as follows.

$$\begin{cases} \hat{V}_{L,1} = \text{conv2D}(\text{avgp}_{s4}(V_{L,1})), \\ \hat{V}_{L,2} = \text{conv2D}(\text{cat}(\hat{V}_{L,1}, \text{avgp}_{s2}(V_{L,2}))), \\ \hat{V}_{L,3} = \text{conv2D}(\text{cat}(\hat{V}_{L,2}, V_{L,3})). \end{cases} \quad (5)$$

The final result is obtained by putting $\hat{V}_{L,3}$ into the detection head. Here, in order to keep consistency of 3D features, the same detection head as our stereo model is used for detection.

Our LiDAR-based model provides multi-scale light-weight voxel features $\hat{V}_{L,i}$ to perform multi scale 3D feature imitation. The multi-scale enhanced light-weight voxel features (\hat{V}_i) in our stereo-based detector have the same shape with the multi-scale light-weight voxel features ($\hat{V}_{L,i}$) in the LiDAR-based detector. Therefore, we could use the following multi scale imitation loss to minimize the feature distances between \hat{V}_i and $\hat{V}_{L,i}$:

$$L_{im} = \sum_{i=1,2,3} \frac{1}{N} \left| M_{fg} M_{sp} (g(\hat{V}_i) - \hat{V}_{L,i}) \right|^2. \quad (6)$$

where i represents the scale, g is a single convolutional layer with kernel size 1, M_{fg} is the foreground mask, M_{sp} is the sparse mask of light-weight LiDAR voxel feature, $N = M_{fg} M_{sp}$ is the normalization factor. and the light-weight LiDAR voxel feature is normalized by the channel-wise expectation of non-zero absolute values.

3.4. Depth Estimation and 3D object Detection

3D Detection Head The multi-scale enhanced light-weight voxel features (\hat{V}_i) are input to a classification head

and a regression head for 3D object detection. For classification, we use Focal loss [16]. For regression, we use a combination of L1 loss and auxiliary rotated 3D IoU loss [42]. In our EGFN, we also employ auxiliary 2D object supervisions on the features F_{l1} out of the backbone following LIGA-Stereo [5]. The features F_{l1} are directly input to an ATSS [41] for 2D detection without being upsampled to full resolution.

Depth head For depth estimation, we upsample layer III of the light-fv₃ to the original resolution, use several convolutions to make aggregation and predict the depth map. GT is the depth map transformed from the GT point cloud. CE loss is adopted to supervise learning the depth map.

4. Experiments

We perform the experiments on the typical KITTI benchmark [4]. The dataset consists of 7,481 training frames and 7,518 test frames. Following the works [14, 20, 33], we split the original training set into the training set and validation set respectively. The training set has 3712 images and the validation set has 3769 images. We train our model on the KITTI training set with 3712 images and evaluate it on the validation set. Moreover, we also train the model in the original training set and test it on the KITTI test set obtaining the final results, which are submitted to the official evaluation benchmark to evaluate the performance of our method.

4.1. Implementation Details

We first train our proposed LiDAR-based model on the KITTI training set. When training the stereo-based model, we run the pre-trained LiDAR-based module to provide the supervision of multi-scale light-weight voxel features and do not update the parameters of the LiDAR-based module. Our method is trained with one NVIDIA RTX 3090 GPU with Adam for optimization. During the training, there are 55 epochs and the learning rate is set as 0.001 for the first 50 epochs, then for the final 5 epochs with a reduced learning rate of 0.0001. The overall training time is about 20 hours.

The detection area is set as [2m, 59.6m] for the Z (depth) axis, [-30m, 30m] for the X axis, and [-1m, 3m] for the Y axis. The voxel sizes of our stereo model and LiDAR detector are set as (0.4m, 0.4m, 0.8m) and (0.05m, 0.05m, 0.1m), respectively.

4.2. Comparison with state-of-the-art methods

We compare our EGFN with several state-of-the-art methods on KITTI benchmark. Tab. 1 presents the comparisons in terms of speed and accuracy AP_{3d} . Comparing with the fast stereo methods of RTS3D [15], YOLOStereo3D [17], SC [30], RT3DStereo [10], and RT3D-GMP [11], the proposed EGFN achieves the best mAP of 46.39 on the test set for moderate levels of car

Method	Time	IoU > 0.7(val)			mAP(test)		
		Easy	Moderate	Hard	Easy	Moderate	Hard
TL-Net [1]	-	18.15	14.26	13.72	7.64	4.37	3.74
Stereo RCNN [14]	300ms	54.11	36.69	31.07	47.58	30.23	23.72
IDA3D [19]	300ms	54.97	37.45	32.23	45.09	29.32	23.13
PL: F-PointNet [33]	400ms	59.4	39.8	33.5	39.70	26.70	22.30
PL: AVOD [33]	400ms	61.9	45.3	39	54.53	34.05	28.25
PL++: AVOD [40]	400ms	63.2	46.8	39.8	-	-	-
PL++: P-RCNN [40]	400ms	62.3	44.9	41.6	61.11	42.43	36.99
OC-Stereo [20]	350ms	64.07	48.34	40.39	55.15	37.60	30.25
ZoomNet [35]	300ms	62.96	50.47	43.63	55.98	38.64	30.97
Disp R-CNN [31]	387ms	64.29	47.73	40.11	68.21	45.78	37.73
DSGN [3]	670ms	72.31	54.27	47.71	73.50	52.18	45.14
CG-Stereo	570ms	76.17	57.82	54.63	74.39	53.58	46.50
LIGA [5]	400ms	84.92	67.06	63.80	81.39	64.66	57.22
RT3DStereo [10]	80ms	-	-	-	29.90	23.28	18.96
Stereo-Centernet [30]	40ms	55.25	41.44	35.13	49.94	31.30	25.62
RTS3D(it=1, re=20) [15]	39ms	63.65	44.5	37.48	58.51	37.38	31.12
RT3D-GMP [11]	60ms	-	-	-	45.79	38.76	30.00
YOLOStereo3d [17]	50ms	72.06	46.58	35.53	65.68	41.25	30.42
Ours	62ms	72.37	54.40	46.50	65.80	46.39	38.42

Table 1. Comparison (AP_{3D}) of some state-of-the-art 3D stereo object (car) detection methods on both KITTI validation and test sets. The inference time, except YOLOStereo3D, is taken from the leaderboards on official KITTI website. YOLOStereo3D and our EFGN are reported on NVIDIA RTX 3090.

Method	Time	IoU > 0.5			IoU > 0.7		
		Easy	Moderate	Hard	Easy	Moderate	Hard
TL-Net [1]	-	62.46	45.99	41.92	29.22	21.88	18.83
Stereo RCNN [14]	300ms	87.13	74.11	58.93	68.50	48.30	41.47
IDA3D [19]	300ms	88.05	76.69	67.29	70.68	50.21	42.93
PL: F-PointNet [33]	400ms	89.8	77.6	68.2	72.8	51.8	44
PL: AVOD [33]	510ms	76.8	65.1	56.6	60.7	39.2	37
PL++: AVOD [40]	400ms	89	77.5	68.7	74.9	56.8	49
PL++: PIXOR [40]	400ms	89.9	75.2	67.3	79.7	61.1	54.5
PL++: P-RCNN [40]	400ms	88.4	76.6	69	73.4	56	52.7
OC-Stereo [20]	350ms	90.01	80.63	71.06	77.66	65.95	51.20
ZoomNet [35]	300ms	90.62	88.40	71.44	78.68	66.19	57.60
Disp R-CNN [31]	387ms	90.67	80.45	71.03	77.63	64.38	50.68
DSGN [3]	670ms	-	-	-	83.24	63.91	57.83
CG-Stereo [13]	570ms	97.04	88.58	80.34	87.31	68.69	65.80
LIGA [5]	400ms	97.22	90.27	88.36	89.35	77.26	69.05
Stereo-Centernet [30]	40ms	-	-	-	71.26	53.27	45.53
RTS3D(it=2, re=10) [15]	39ms	90.41	78.70	70.03	76.56	56.46	48.20
YOLOStereo3d [17]	50ms	96.52	79.62	62.50	80.69	55.22	43.47
Ours	62ms	89.95	79.81	70.59	79.24	65.42	57.11

Table 2. Comparison (AP_{BEV}) of some state-of-the-art 3D object (car) detectors on KITTI validation set. The inference time, except YOLOStereo3D, is taken from the leaderboards on official KITTI website. YOLOStereo3D and ours are reported on NVIDIA RTX 3090.

class. YOLOStereo3D [17] has the best performance in all existing fast methods with the speed is 50ms per frame (test on NVIDIA RTX 3090) and accuracy being 41.25. Our method outperforms YOLOStereo3D by an absolute gain of 5 % at the speed of 62ms per frame. Our EFGN outperforms ZoomNet [35], Disp R-CNN [31], OC-Stereo [20] and PL++: PIXOR [40] with a more than 6-fold speedup.

Tab. 2 shows the comparisons in terms of both speed and accuracy AP_{bev} . Our EFGN achieves the best trade-off between the speed and the precision. We further show some qualitative results of 3D object detection in Fig. 6.

4.3. Ablation Study

In this subsection, we conduct the adequate ablation study to verify the effectiveness of different modules in our EFGN. All the results in this section are evaluated on validation set using KITTI metric with 40 recall values.

EGFR As shown in Tab. 3, the accuracy of our EFGN without multi-scale 3D feature imitation is already 49.69, which is the best in all fast method. It demonstrates that our EFGN can improve 3D features to reduce the gap between the fast stereo methods and the high-precision meth-

Method			IoU > 0.7		
Basic Block	en light-fv	en V_i	Easy	Moderate	Hard
✓			57.12	37.87	31.52
✓	✓		64.98	46.24	38.79
✓		✓	63.05	45.18	38.85
✓	✓	✓	68.05	49.69	41.40

Table 3. The performance of EGFR. ‘basic-block’ denotes only the basic block layer III, ‘en light-fv’ denotes Multi-scale enhancement on the light-fv, and ‘en V_i ’ denotes multi-scale Geometry feature enhancement on the V_i .

Method	IoU > 0.7		
	Easy	Moderate	Hard
SECOND [36]	88.82	78.57	77.40
our LiDAR detector	91.01	81.23	78.64

Table 4. Result of our proposed teacher LiDAR module. Compared with our baseline SECOND .

Method	IoU > 0.7		
	Easy	Moderate	Hard
No Imitation	68.05	49.69	41.40
Imitation	72.25	51.40	43.11
Multi-Scale IM	72.44	52.33	43.74

Table 5. Comparison of different imitation strategy. ‘Multi-Scale IM’ denotes multi-scale 3D features imitation.

ods. Only using one basic block in the EGFR module (*i.e.* layer III) obtains 37.87 AP on the Moderate set. After we employ multi-scale enhancement on the three basic blocks to construct the enhance light-fv, the accuracy will improve to 46.45 AP, which demonstrates that it is essential to carry out multi scale enhancement.

New teacher LiDAR model We propose a new teacher LiDAR-based model with high accuracy of 81.23 AP on the moderate set, which is higher than that of the baseline network SECOND in [36] as shown in Tab. 4. It provides light-weight voxel features that are consistent with the multi-scale light-weight voxel features of our model.

Mult-scale 3D feature imitation Based on our EGFR module, we add the teacher LiDAR-based model to provide 3D features for multi scale distillation. Different from distillation strategy in [5], we not only supervise the last 3D geometry features, but also supervise multi-scale intermediate features in the process of obtaining the last 3D geometry feature. As shown in Tab. 5, compared with only supervising the last 3D features, our multi-scale supervision improves 1%. Our proposed new distillation method can help our stereo-based model learn 3D geometry feature

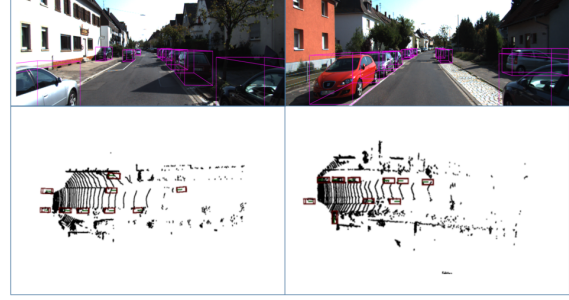


Figure 6. Qualitative results of Stereo 3D object detection. The upper part is detection result in image viewpoint, and the lower part is detection result in BEV.

Method			IoU > 0.7		
V	\hat{V}	Muti-scale IM	Easy	Moderate	Hard
✓			64.63	46.45	38.92
✓	✓		68.05	49.69	41.40
✓	✓	✓	72.43	52.33	43.74

Table 6. Impact of integrating the proposed modules on KITTI validation set. ‘V’ denotes light-weight voxel feature, ‘ \hat{V} ’ denotes enhanced light-weight voxel feature, and ‘Muti-scale IM’ denotes multi-scale 3D features imitation.

better.

Integration of different modules Tab. 6 shows the impacts of integrating the proposed modules including light-weight voxel features V_i (obtained from EGFR without multi-scale enhancement in 3D space), enhanced light-weight voxel features \hat{V}_i (out from complete EGFR module), and multi-scale 3D features distillation. On the moderate subset, the accuracy of the model with light-weight voxel features V_i is 46.45. The enhanced light-weight voxel features \hat{V}_i provides an absolute gain of 3.24% and multi-scale 3D feature imitation achieves an absolute gain of 2.64%.

5. Conclusion

In this paper, we have proposed an efficient geometry feature network for stereo 3D object detection. An efficient 3D geometry feature representation module is designed to learn better 3D features significantly improving the accuracy of stereo 3D object detection with negligible overheads. We have also designed a new multi-scale knowledge distillation method to guide the efficient geometry features learning. It is concluded that our proposed method achieves an AP_{3d} improvement of 5% on the official KITTI benchmark at the speed of 62ms compared with the best fast method available. Our EGFR achieves a better trade-off between accuracy and speed.

References

- [1] Xiaozhi Chen, Kaustav Kundu, and Y. Zhu. Triangulation learning network: From monocular to stereo 3d object detection. *Proc. International Conference on Neural Information Processing Systems, MIT Press*, 2019. 7
- [2] Yilun Chen, Shu Liu, Xiaoyong Shen, and Jiaya Jia. Fast point r-cnn. *Proc. IEEE International Conf. Computer Vision.*, 2019. 3
- [3] Yilun Chen, Shu Liu, Xiaoyong Shen, and Jiaya Jia. Dsgn: Deep stereo geometry network for 3d object detection. *Proc. IEEE Conference on Computer Vision and Pattern Recognition.*, 2020. 1, 2, 3, 4, 7
- [4] Andreas Geiger, Philip Lenz, and Raquel Urtasun. Are we ready for autonomous driving? the kitti vision benchmark suite. *Proc. IEEE Conference on Computer Vision and Pattern Recognition*, 2012. 1, 6
- [5] Xiaoyang Guo, Shaoshuai Shi, Xiaogang Wang, and Hongsheng Li. Liga-stereo: Learning lidar geometry aware representations for stereo-based 3d detector. *Proc. IEEE International Conf. Computer Vision*, 2021. 1, 2, 3, 6, 7, 8
- [6] Chenhang He, Hui Zeng, Jianqiang Huang, Xian-Sheng Hua, and Lei Zhang. Structure aware single-stage 3d object detection from point cloud. *Proc. IEEE Conference on Computer Vision and Pattern Recognition.*, 2020. 3
- [7] Kaiming He, Xiangyu Zhang, Shaoqing Ren, and Jian Sun. Deep residual learning for image recognition. *Proc. IEEE International Conf. Computer Vision*, 2016. 3, 4
- [8] Byeongho Heo, Jeessoo Kim, Sangdoo Yun, Hyojin Park, Nojun Kwak, and Jin Young Choi. A comprehensive overhaul of feature distillation. *Proc. IEEE International Conf. Computer Vision.*, 2019. 3
- [9] Geoffrey Hinton, Oriol Vinyals, and Jeff Dean. Distilling the knowledge in a neural network. *arXiv*, 2015. 3
- [10] H. Königshof, N. Salscheider, and C. Stiller. Realtime 3d object detection for automated driving using stereo vision and semantic information. *Proc. International IEEE Conference on Intelligent Transportation Systems*, 2019. 1, 3, 6, 7
- [11] H. Königshof, N. Salscheider, and C. Stiller. Learning-based shape estimation with grid map patches for realtime 3d object detection for automated driving. *Proc. International IEEE Conference on Intelligent Transportation Systems*, 2020. 1, 3, 6, 7
- [12] Alex H. Lang, Sourabh Vora, Holger Caesar, Lubing Zhou, Jiong Yang, and Oscar Beijbom. Pointpillars: Fast encoders for object detection from point clouds. *Proc. IEEE Conference on Computer Vision and Pattern Recognition.*, 2019. 3
- [13] C. Li, J. Ku, and S. L. Waslander. Confidence guided stereo 3d object detection with split depth estimation. *Proc. IEEE/RSJ International Conference on Intelligent Robots and Systems*, 2020. 4, 7
- [14] Peiliang Li, Xiaozhi Chen, and Shaojie Shen. Stereo r-cnn based 3d object detection for autonomous driving. *Proc. IEEE Conference on Computer Vision and Pattern Recognition*, 2019. 1, 3, 6, 7
- [15] Peixuan Li, Shun Su, and Huaici Zhao. Rts3d: Real-time stereo 3d detection from 4d feature-consistency embedding space for autonomous driving. *Proc. AAAI Conference on Artificial Intelligence*, 2021. 3, 6, 7
- [16] Tsung-Yi Lin, Priya Goyal, Ross Girshick, Kaiming He, and Piotr Dollár. Focal loss for dense object detection. *arXiv*, 2017. 6
- [17] Yuxuan Liu, Lujia Wang, and Ming Liu. Yolostereo3d: A step back to 2d for efficient stereo 3d detection. *Proc. International Conference on Robotics and Automation*, 2021. 1, 2, 3, 6, 7
- [18] W. Luo, A. G. Schwing, and R. Urtasun. Efficient deep learning for stereo matching. *Proc. IEEE Conference on Computer Vision and Pattern Recognition.*, 2016. 4
- [19] Peng Wanli Peng, Hao Pan, He Liu, and Yi Sun. IDA-3D : Instance-depth-aware 3d object detection from stereo vision for autonomous driving. *Proc. IEEE Conference on Computer Vision and Pattern Recognition*, 2020. 1, 3, 7
- [20] Alex D. Pon, Jason Ku, Chengyao Li, and Steven L. Waslander. Object-centric stereo matching for 3d object detection. *Proc. IEEE International Conference on Robotics and Automation*, 2020. 1, 3, 6, 7
- [21] Charles R. Qi, Or Litany, Kaiming He, and Leonidas J. Guibas. Deep hough voting for 3d object detection in point clouds. *Proc. IEEE International Conf. Computer Vision*, 2019. 3
- [22] Charles R. Qi, Hao Su, Kaichun Mo, and Leonidas J. Guibas. Pointnet: Deep learning on point sets for 3d classification and segmentation. *Proc. IEEE Conference on Computer Vision and Pattern Recognition*, 2017. 1, 3
- [23] Charles R. Qi, Li Yi, Hao Su, and Leonidas J. Guibas. Pointnet++: Deep hierarchical feature learning on point sets in a metric space. *Proc. International Conference on Neural Information Processing Systems*, 2017. 1, 3
- [24] Adriana Romero, Nicolas Ballas, Samira Ebrahimi Kahou, Antoine Chassang, Carlo Gatta, and Yoshua

- Bengio. Fitnets: Hints for thin deep nets. *ICLR*, 2015. 3
- [25] Shaoshuai Shi, Chaoxu Guo, Li Jiang, Zhe Wang, Jianping Shi, Xiaogang Wang, and Hongsheng Li. Pvrnn: point-voxel feature set abstraction for 3d object detection. *Proc. IEEE Conference on Computer Vision and Pattern Recognition.*, 2019. 3
- [26] Shaoshuai Shi, Xiaogang Wang, and Hongsheng Li. Pointtrcnn: 3d object proposal generation and detection from point cloud. *Proc. IEEE Conference on Computer Vision and Pattern Recognition*, 2019. 1
- [27] Shaoshuai Shi, Xiaogang Wang, and Hongsheng Li. Pointtrcnn: 3d object proposal generation and detection from point cloud. *Proc. IEEE Conference on Computer Vision and Pattern Recognition.*, 2019. 3
- [28] Shaoshuai Shi, Zhe Wang, Jianping Shi, Xiaogang Wang, and Hongsheng Li. From points to parts: 3d object detection from point cloud with part aware and part-aggregation network. *IEEE TPAMI*, 2020. 3
- [29] Weijing Shi and Ragunathan (Raj)Rajkumar. Pointgcn: Graph neural network for 3d object detection in a point cloud. *Proc. IEEE Conference on Computer Vision and Pattern Recognition.*, 2020. 3
- [30] Yuguang Shi, Yu Guo, Zhenqiang Mi, and Xinjie Li. Stereo centernet based 3d object detection for autonomous driving. *arXiv:2103.11071*, 2021. 1, 3, 6, 7
- [31] Jiaming Sun, Linghao Chen, Yiming Xie, Siyu Zhang, Qinhong Jiang, Xiaowei Zhou, and Hujun Bao. Disp r-cnn: Stereo 3d object detection via shape prior guided instance disparity estimation. *Proc. IEEE Conference on Computer Vision and Pattern Recognition*, 2020. 1, 3, 6, 7
- [32] Q. Wang, S. Shi, S. Zheng, K. Zhao, and X. Chu. Fadnet: A fast and accurate network for disparity estimation. *arXiv*, 2020. 4
- [33] Yan Wang, Wei-Lun Chao, Divyansh Garg, Bharath Hariharan, Mark Campbell, and Kilian Q. Weinberger. Pseudo-lidar from visual depth estimation: Bridging the gap in 3d object detection for autonomous driving. *Proc. IEEE Conference on Computer Vision and Pattern Recognition*, 2019. 1, 3, 6, 7
- [34] Qian Xie, Yu-Kun Lai, Jing Wu, Zhoutao Wang, Yiming Zhang, Kai Xu, and Jun Wang. Mlcvnet: Multi-level context votenet for 3d object detection. *Proc. IEEE Conference on Computer Vision and Pattern Recognition*, 2020. 3
- [35] Zhenbo Xu, Wei Zhang, Xiaoqing Ye, Xiao Tan, Wei Yang, Shilei Wen, Errui Ding, Ajin Meng, and Liusheng Huang. Zoomnet: Part-aware adaptive zooming neural network for 3d object detection. *Proc. AAAI Conference on Artificial Intelligence*, 2020. 3, 7
- [36] Yan Yan, Yuxing Mao, and Bo Li. Second: Sparsely embedded convolutional detection. *Sensors*, 2018. 8
- [37] Zetong Yang, Yanan Sun, Shu Liu, and Jiaya Jia. 3dssd: Point-based 3d single stage object detector. *Proc. IEEE Conference on Computer Vision and Pattern Recognition.*, 2020. 3
- [38] Zetong Yang, Yanan Sun, Shu Liu, Xiaoyong Shen, and Jiaya Jia. Std: Sparse to-dense 3d object detector for point cloud. *Proc. IEEE International Conf. Computer Vision.*, 2019. 3
- [39] Maosheng Ye, Shuangjie Xu, and Tongyi Cao. Hvnet: Hybrid voxel network for lidar based 3d object detection. *Proc. IEEE Conference on Computer Vision and Pattern Recognition.*, 2020. 3
- [40] Yurong You, Yan Wang, Wei-Lun Chao, Divyansh Garg, Geoff Pleiss, Bharath Hariharan, Mark Campbell, and Kilian Q. Weinberger. Pseudo-lidar++: Accurate depth for 3d object detection in autonomous driving. 2020. *Proc. International Conference on Learning Representations*, 2020. 1, 3, 7
- [41] Shifeng Zhang, Cheng Chi, Yongqiang Yao, Zhen Lei, and Stan Z. Li. Bridging the gap between anchor-based and anchor-free detection via adaptive training sample selection. *Proc. IEEE Conference on Computer Vision and Pattern Recognition*, 2020. 6
- [42] Dingfu Zhou, Jin Fang, Xibin Song, Chenye Guan, Junbo Yin, Yuchao Dai, and Ruigang Yang. Iou loss for 2d/3d object detection. In *International Conference on 3D Vision (3DV)*, 2019. 6
- [43] Yin Zhou and Oncel Tuzel. Voxelnet: End-to-end learning for point cloud based 3d object detection. *Proc. IEEE Conference on Computer Vision and Pattern Recognition.*, 2018. 3